Canadian Science Publishing | Canadian Journal of Physics

Dynamical and Optimal Procedure to Analyse the Exhibition of Physical Attribute Imparted by Sutterby Magneto Nano Fluid in Darcy medium yield by Axially Stretched Cylinder

Journal:	*Canadian Journal of Physics*
Manuscript ID	cjp-2018-0581.R2
Manuscript Type:	Article
Date Submitted by the Author:	28-Dec-2018
Complete List of Authors:	Bilal, S.; AIR University Islamabad Sohail, M.; Institute of Space Technology Naz, R.; Institute of Space Technology Malik, M.Y.; King Khalid University
Keyword:	Sutterby Fluid, Optimal Analysis, Dynamical Analysis, Darcy Law, Magnetic field
Is the invited manuscript for consideration in a Special Issue? :	Not applicable (regular submission)

Dynamical and Optimal Procedure to Analyze the Exhibition of Physical Attribute Imparted by Sutterby Magneto Nanofluid in Darcy medium yield by Axially Stretched Cylinder

S. Bilal[1*], M. Sohail[2], R. Naz[2] and M. Y. Malik[3,4]

[1]Department of Mathematics, AIR University, Sector E-9 Islamabad *P.O.Box* 44000, Pakistan

[2]*Department of Applied Mathematics and Statistics, Institute of Space Technology P.O.Box* 2750*, Islamabad* 44000*, Pakistan*

[3]Department of Mathematics, King Khalid University P.O. Box 3236 Abha, 61413 Saudi Arabia

[4]Department of Mathematics, Quaid-i-Azam University, Islamabad *P.O.Box* 44000, Pakistan

Abstract: Current exertion is executed to interpret the heat and mass transmission of Sutterby fluid by conferring scintillating aspects of magnetic field. Flow field equations in cylindrical coordinates are attained by incorporating **Darcy** resistance law. Afterwards, mathematical structure regarding the physical problem is formulated. This formulation yields intricate nonlinear set of partial differential expressions. A suitable scaling group of variables is employed on consequent equations to transfigure them in non-dimensional form. Dynamical and optimal analysis (OHAM) are performed to achieve physical features of present problem from the solution. Graphical depiction is offered and illustrated for the flow behavior of convoluted physical parameters on velocity, temperature and concentration profiles. Additionally, the quantities (local shear stress coefficient, thermal convective transfer coefficient and local mass flux coefficient in limiting case) which are responsible to extract out the physical phenomena in the vicinity of stretched surface are computed and demarcated by varying controlling flow parameters.

Keywords: Sutterby nanofluid; **Darcy** resistance; OHAM; nonlinear dynamical analysis; stretching cylinder.

1 Nomenclature

T^*_∞	Ambient temperature	M	Magnetic parameter
C^*_∞	Ambient concentration	Pr	Prandtl number
D^*_B	Brownian diffusion coefficient	U_o	Reference velocity
N^*_B	Brownian motion parameter	R	Radius of cylinder
C^*	Concentration	$\widetilde{\tau}$	Ratio of heat capacity
b^2	Consistency index	B_0	Strength of magnetic field
γ	Curvature of cylinder	Sc	Schmidt number
ρ	Density of fluid	λ	Sponginess parameter
Υ_2	Darcy resistance parameter	c_p	Specific heat
ξ	Dimensionless independent variable	Υ_1	Sutterby nanofluid parameter
θ	Dimensionless temperature	T^*_w	Temperature of wall
ϕ	Dimensionless concentration	K^*	Thermal conductivity
f'	Dimensionless velocity	$\widetilde{E^{*t}_m}$	Total squared residuals errors
$\hat{C}^D_F$	Dimensionless skin friction coefficient	T^*	Temperature
$\hat{S}^D_u$	Dimensionless mass flux coefficient	α	Thermal diffusivity
$\hat{N}^D_u$	Dimensionless heat transfer coefficient	u	Velocity component in $r-$ direction
σ	Electrical conductivity	w	Velocity component in $z-$ direction
ε	Flow comportment index	$U_w(z)$	Velocity of wall

2 Introduction

Researcher has announced present time to be technology driven era due to high profiled demand of industrial production. So the motivated researchers are taking immense interest to increase the large scale productivity. Researchers have also acknowledged through various experimental schemes and procedures about the fact that productivity enhancement of industrial sector heavily depends on withal thermal transferal abilities of materials. Usually thermal features in large scale products are accessed through common fluids but limited thermal aptitudes have implemented reservations on their utilization. To achieve the required purpose researchers have conducted several thought provoking experimental investigation to sort out the solution of such salient problem. At last they came up with the decision that thermal capabilities of materials can be improved by enhancing thermal conductance of material. They also floated the idea that thermal conductance is improved by incorporating small sized fluid particles in to host fluid particles. Consequently addition of small sized particles in carrier fluid was inaugurated by Choi [1]. He termed these particles to nanoparticles on behalf of their composite structure sizes and named this field as nanotechnology. Afterwards several enthusiastic researchers have followed his work and discussed about various nanoparticles and their thermal conductance. Masuda et al. [2] estimated the disparities in both thermal conductivity and the viscosity of conventional fluids by the dispersal of ultrafine particles in host fluid. Buongiorno [3] did seminal work on nanofluid by presenting speculative model in order to interrogate the thermal features of carrier fluids. He contemplated that the improvement in conductance of regular fluid is due to low volume fraction and small size of added nanoelements. Actually, nanotechnology is of generous significance in

numerous fields namely transportation, metallurgical and chemical devices, manufacturing of micro scale objects, generation of power, cancer patients therapy etc. Nield and Kuznetsov [4] capitalized Buongiorno model to adumbrate convective heat transfer induced by vertically stretched surface immersed in **Darcy** medium. They instituted that strength of heat transfer rate decreases by escalating Brownian motion and thermophoresis parameters. **Some recent studies relevant to nanofluid flow can be found in [5 – 7]. Sheikholeslami et al. [8] studied water based nanofluid turbulent flow and entropy generation in a heat exchanger by utilizing Finite volume technique. In order to upsurge the heat transfer rate, belt turbulators perverted into the tube are inserted. Second-law is presented for different values of height ratio and pitch ratio and Reynolds number Associated formulas for entropy generation and Bejan number are provided in their study. Their findings indicate that the secondary current upsurges with growing number of revolutions. Increase in Bejan number and total entropy generation with increase in pitch ratio is noticed. In another study Sheikholeslami et al. [9] employed CVFEM to explore convective heat transfer of magnetohydrodynamic alumina nanofluid in a permeable enclosure. Impact of different influential variables are displayed graphically. Displayed results depicts that Lorentz forces upsurges the heating mechanism.** The investigation on nanofluid flow over linearly stretched sheet was primarily initiated by Khan and Pop [10] . They numerically investigated the impact of thermophoretic force and Brownian movement of nanostructures on thermal conductivity of fluid. The collective heat and mass features over permeable exponentially stretched surface with second order slip was discussed by Rahman et al. [11]. Radiative heat transfer of nanofluid with variant surface heat flux and effects of chemically reacting species are demonstrated by Zhang et al. [12]. Nadeem et al. [13] performed numerical analysis of magnetohydrodynamic flow of Maxwell fluid past a stretching sheet in the attendance of nanoparticles. Malik et al. [14] constructed computational study to explore the effects of nanoparticles on Eyring-Powel fluid model. Raju and Sandeep [15] addressed thermal and concentration transport due to Casson nanofluid in rotating frame. Nadeem and Saleem [16] performed comprehensive homotopy analysis to anticipate the impact of higher grade nanofluid over a rotatory cone. Raju et al. [17] conducted comparative study to evaluate the fabulous enhancement in host fluid by considering various types of metallic nanostructures. He also depicted the collaborated effects of temperature dependent viscosity. Few recent studies are encountered to explore the characteristics of nanofluid in [18 – 30].

Engineers and scientists have observed experimentally about the transporting abilities of fluids. Thus they have recognized the fact that dynamical transport mechanism all around the world can be best explained by the fluid rheology. Transport processes in some walks of discipline are simple in nature and can be interpreted by a linear expression among the stain and stress. But Navier addresses the concept that most of technological and industrial productive projects (Polymer melting, certain oils and greases, claying and other suspensions, drilling mud etc.) involve complex transport procedures. Therefore mentioned materials exhibit a non-empirical strain-stress. Such type of fluids which represents an intricate nonlinear **constitutive** stress strain relationship is renowned as non-Newtonian fluids. There are various application of non-Newtonian fluids e.g. in electronic devices, analytical instrumentation, medicine, friction reducing agent, angular momentum change agent, heat transfer agent etc. So for better physical description of such type of fluids these are classified into pseudoplastic fluids, dilatant fluids and thixotropic fluids. In recent years several fluid models are proposed which explain the dual properties of pseudoplastic and dilatant materials. Among these is

Sutterby fluid model [31]. Guha and Pradahan [32] investigated convective boundary layer flow of Sutterby fluid over an isothermal horizontal plate. Bijjan et al. [33] illustrated thermal transport within laminar flow of dilatant power law fluid past through cylinder. Azhar et al. [34] exposed the stagnant Sutterby nanofluid flow with entropy generation numerically. Hayat et al. [35] explored the radiative effect on peristaltic Sutterby fluid flow in vertical channel. Xie and Jian [36] described the power law magnetohydrodynamics fluid flow through micro-parallel rotating channel. Hayat et al. [37] disclosed the peristalsis analysis of Sutterby liquid flow through porous medium. In another survey Hayat et al. [38] exhibited the impact of wall properties on peristalsis of radiative Sutterby fluid flow in curved surface.

Coupling of magnetic field with fluid mechanics is declared as magnetic field dynamics (MFD) and such interacting fluids are called as electrically conducting fluids. The dynamics of the magnetic field flows (MFF) has received pervasive attention of enthusiastic researchers due to overwhelming applications in various naturally occurring phenomenons like geophysics, astronomical physics and in the movement of earth mantle. In extension, the flow problems with magnetic field features is endorsed by various researchers due its applications in engineering and modern industry namely plasma confinement, solar physics, cosmic fluid dynamics, and many more. Furthermore, the experimental analyst has also observed that appliance of external magnetic field to the fluid flows induces both electric and magnetic field. Due to low magnetic Reynold assumption the induced electric field is neglected and thus as a net amount induced magnetic field retains. This produced magnetic field is of extreme importance for realistic depiction of fluid flow analysis. Few initial studies regarding electrically conducting fluid flows in various geometrical conditions were disclosed by following authors. For sake of brevity here few are mentioned. Pavlov [39] identified features of magnetohydrodynamic flow in the light of linearly deformed sheet. They extracted exact solution of problem to depict out the influence of magnetic field on momentum of fluid flow. In this frame as far as cylindrical coordinates are concerned, Ishak et al. [40] implemented implicit finite difference (Keller box) scheme to recognize the impact of magnetic field on fluid flow due to a stretchable cylinder. Afterwards, following the above mentioned initial work in this field new researchers have acknowledged the fact the study of fluid flows with magnetic field is highly aimful. Thus they are now concentrating their intentions towards magnetohydrodynamic flows. In this regards a lot of studies are conducted but few of them are as follows. **Sheikholeslami and Rokni [41]discussed the influence of external magnetic source on Fe3O4-water in a cavity by utilizing CVFEM. They noticed that velocity decreases by augmenting the values of magnetic parameter.** Makinde and Mutuku [42] investigated the hydromagnetic thermal boundary layer of nanofluid over a convectively heated flat plate with viscous dissipation and Ohmic heating effects. **Impact of variable magnetic field on flow of nanofluid with heat transfer is reported by Sheikholeslami and Vajravelu [43].** Singh and Makinde [44 − 45] anticipated magnetohydrodynamic boundary layer flow over an inclined stretching sheet under volumetric heat generation phenomenon and later on they extended previous finding to reveal isothermal slip flow induced by vertically stretched cylinder. Das et al. [46] examined magnetohydrodynamic flow over linearly deformed sheet and also accounted momentum slip phenomenon. Mukhopaday et al. [47] proved the claim regarding suppressing attribute of magnetic field on velocity by conducting study on cylindrical geometry. Qasim et al. [48] retreated slip flow effect along a cylindrical stretching surface under prescribed heat flux. It was found that the magnitude of percent difference for heat transfer rate regarding magnetic nanoparticles decreases by enhancing magnetic field strength. Malik et al. [49] considered flow of tangent hyperbolic fluid along a cylindrical stretched surface under magnetic field effect. They reconfirmed the magnetic field effects

and presented interesting results. Recently, Benazir et al. [50] examined the magnetic field bearings for unsteady Casson fluid flow over a vertical cone and flat surface (plate) under heat source/sink effect.

In views of practical applications in many fields of applied science, the aim of current exploration is to venture supplementary in the regime of heat and mass transference for the rheology of magnetohydrodynamic flow of Sutterby nanofluid model with the addition of **Darcy** resistance in stretching cylinder. Existing literature witness that no study in past is made in this direction, so present attempt is to explore it via utilizing optimal homotopy analysis scheme $[51-54]$ is functioned for the exceptional convergence benchmarks for governing dimensionless equations. Various graphs are prepared to show the real insight of the considered research.

3 Problem Structure

3.1 Model statement

The steady, laminar 2-D, incompressible boundary layer flow of Sutterby nanofluid in the presence of Darcy resistance [31] **is considered. Furthermore, magnetic field is applied along** $r-$ **direction perperpendicular to the fluid flow along** $z-$ **direction. Induced magnetic field is not considered subject to small magnetic Reynold number and as well as effects of electric field are not taken into interpretation.**

$$R = -\frac{\mu}{2k^*}\left[\frac{\sinh^{-1}(b\bar{\gamma})}{b\bar{\gamma}}\right]^{\varepsilon}\overrightarrow{V}. \tag{1}$$

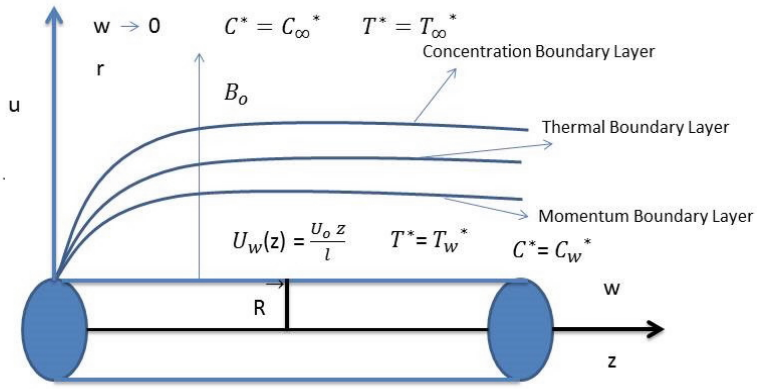

Fig. **1** Portrayal for physical happening.

Flow is considered in cylinder that is stretched with velocity $U_w(z)$. Constant temperature (T_w^*) and concentration (C_w^*) are assumed at the surface of cylinder. Undeviating magnetic field of strength (B_0) is imposed in the vertical direction to flow. Heat and mass transport mechanisms are modelled by using the Fourier and Fick's law respectively. Nanofluid model consists of Brownian motion and thermophoresis aspects. With such deduction the prevailing boundary layer equations that designates the physical happening are listed as:

3.1.1 Continuity equation

It is based upon the conservation of mass principle

$$\frac{\partial u}{\partial r}+\frac{u}{r}+\frac{\partial w}{\partial z}=0, \tag{2}$$

3.1.2 Equation of motion

It is based on Newton's 2nd law of motion

$$u\frac{\partial w}{\partial r}+w\frac{\partial w}{\partial z}=\frac{\nu^*}{2}\frac{\partial^2 w}{\partial r^2}+\frac{\nu^*}{2r}\frac{\partial w}{\partial r}-\frac{\nu^*\varepsilon b^2}{4}\left(\frac{\partial w}{\partial r}\right)^2\frac{\partial^2 w}{\partial r^2}-\frac{\sigma B_0^2}{\rho}w+\frac{R_z}{\rho}, \tag{3}$$

3.1.3 Energy equation

It is based upon the first law of thermodynamics

$$u\frac{\partial T^*}{\partial r}+w\frac{\partial T^*}{\partial z}=\frac{K^*}{(\rho c_p)_f}\left[\frac{\partial^2 T^*}{\partial r^2}+\frac{1}{r}\frac{\partial T^*}{\partial r}\right]+\widetilde{\tau}\left[D_B^*\frac{\partial C^*}{\partial r}\frac{\partial T^*}{\partial r}+\frac{D_{T^*}^*}{T_\infty^*}\left(\frac{\partial T^*}{\partial r}\right)^2\right], \tag{4}$$

3.1.4 Species equation

$$u\frac{\partial C^*}{\partial r}+w\frac{\partial C^*}{\partial z}=D_B^*\left[\frac{\partial^2 C^*}{\partial r^2}+\frac{1}{r}\frac{\partial C^*}{\partial r}\right]+\frac{D_{T^*}^*}{T_\infty^*}\left[\frac{\partial^2 T^*}{\partial r^2}+\frac{1}{r}\frac{\partial T^*}{\partial r}\right]. \tag{5}$$

The significant boundary conditions are settled by consuming no slip theory

$$\begin{aligned} u=0,\ w=U_w(z)=\frac{U_0 z}{l},\ T^*=T_w^*,\ C^*=C_w^*\ \text{at}\ r=R,\\ w\to 0,\ C^*\to C_\infty^*,\ T^*\to T_\infty^*\ \text{as}\ r\to\infty. \end{aligned} \tag{6}$$

In the above expressions (u) and (w) are velocity components in $r-$ and $z-$directions respectively, (ε) the flow comportment index, (b^2) the consistency index, (T^*) and (C^*) the temperature and concentration respectively, (T_∞^*) the ambient temperature, (C_∞^*) the ambient concentration, (ρ) the density, (c_p) the specific heat, (K^*) the thermal conductivity, $(\widetilde{\tau})$ the ratio of operative heat capability of the nanoparticle material to heat capability of fluid, (D_B^*) the Brownian dissemination and $(D_{T^*}^*)$ is thermophoresis diffusion coefficient.

Assuming the following similarity transmutations

$$\begin{aligned} u=-\sqrt{\frac{\nu^* U_0}{l}}\frac{R}{r}f(\xi),\ w=\frac{U_0 z}{l}f'(\xi),\ \xi=\sqrt{\frac{U_0}{\nu^* l}}\left(\frac{r^2-R^2}{2R}\right),\\ \theta(\xi)=\frac{T^*-T_\infty^*}{T_w^*-T_\infty^*},\ \phi(\xi)=\frac{C^*-C_\infty^*}{C_w^*-C_\infty^*}, \end{aligned} \tag{7}$$

Eqs. (3), (4) and (5) takes the form

$$(1+2\gamma\xi)f'''+2ff''-2(f')^2-\frac{\Upsilon_1}{2}(1+2\gamma\xi)^2(f'')^2f'''+\gamma f''-\left(M+\frac{\lambda}{2}\right)f'+\frac{1}{12}\Upsilon_2 f'(f'')^2=0, \tag{8}$$

$$\frac{1}{\mathrm{Pr}}(1+2\gamma\xi)\theta''+\frac{1}{\mathrm{Pr}}f\theta'+(1+2\gamma\xi)\left[N_B^*\theta'\phi'+N_{T^*}^*(\theta')^2\right]=0, \tag{9}$$

$$(1+2\gamma\xi)\phi'' + \gamma\phi' + Scf\phi' + \frac{N_{T^*}^*}{N_B^*}\left[(1+2\gamma\xi)\theta'' + \gamma\theta'\right] = 0, \tag{10}$$

with boundary conditions Eq. (6)

$$\begin{aligned} f &= 0,\ f' = 1,\ \theta = 1,\ \phi = 1 \text{ at } \xi = 0, \\ f' &\to 0,\ \theta \to 0,\ \phi \to 0 \text{ as } \xi \to \infty. \end{aligned} \tag{11}$$

In above expressions (U_0) is the reference velocity, (ν^*) the kinematic viscosity, (ξ) the independent variable, (R) the cylinder radius, (σ) the electrical conductivity, $\gamma = \frac{1}{R}\sqrt{\frac{\nu^* l}{U_0}}$ the curvature parameter, $\Upsilon_1 = \frac{\varepsilon b^2 U_0^3 z^2}{l^3 \nu^*}$ the Sutterby nanofluid parameters, $\Upsilon_2 = \frac{\varepsilon b^2 U_0^2 z^2}{l^2 k^*}$ the **Darcy** resistance parameter, $M = \frac{l\sigma B_0^2}{U_0 \rho}$ the magnetic parameter, $\Pr = \frac{\nu^*}{\alpha}$ the Prandtl number, $Sc = \frac{\nu^*}{D_B^*}$ the Schmidt number, $\lambda = \frac{\nu^* l}{k^* U_0}$ the sponginess parameter, $N_B^* = \frac{\widetilde{\tau} D_B^* (C_w^* - C_\infty^*)}{\nu^*}$ and $N_{T^*}^* = \frac{\widetilde{\tau} D_{T^*}^* (T_w^* - T_\infty^*)}{\nu^* T_\infty^*}$ are Brownian motion and thermophoresis parameters respectively.

4 Nonlinear dynamical analysis

The equivalent system of first order differential equations corresponding to Eqs. (8) - (10) are expressed by assuming $f = y_1$, $f' = y_2 = y_1' = F$, $f'' = y_3 = y_2' = G$, $f''' = y_3' = H$, $\theta = y_4$, $\theta' = y_4' = y_5 = K$, $\theta'' = y_5' = L$, $\phi = y_6$, $\phi' = y_6' = y_7 = M$ and $\phi'' = y_7' = N$ as follows

$$y_3' = \frac{1}{\left[(1+2\gamma\xi) - \frac{\Upsilon_1}{2}(1+2\gamma\xi)^2 (y_3)^2\right]}\left[2(y_2)^2 - 2y_1 y_3 - \gamma y_3 + \left(M + \frac{\lambda}{2}\right) y_2 - \frac{1}{12}\Upsilon_2 y_2 (y_3)^2\right], \tag{12}$$

$$y_5' = -\frac{1}{[(1+2\gamma\xi)]}\left[\gamma y_5 - \Pr(1+2\gamma\xi)\left\{N_B^* y_5 y_7 + N_{T^*}^* (y_5)^2\right\} + \Pr y_1 y_5\right], \tag{13}$$

$$y_7' = -\frac{1}{[(1+2\gamma\xi)]}\left[\gamma y_7 + \frac{N_{T^*}^*}{N_B^*}\left\{(1+2\gamma\xi) y_5' + \gamma y_5\right\} + Sc y_1 y_7\right]. \tag{14}$$

For the dynamical analysis one of the fixed points for the transformed system of ordinary differential equations $y_1' = y_2$, $y_2' = y_3$, $y_4' = y_5$, $y_6' = y_7$ and Eqs. (12) - (14) is $\tilde{O}(0,\ 0,\ 0,\ 0,\ 0,\ 0,\ 0)$. The corresponding Jacobian matrix $\widetilde{\chi} = \widetilde{\chi}(y_1,\ y_2,\ y_3,\ y_4,\ y_5,\ y_6,\ y_7)$ is given as

$$\widetilde{\chi} = \begin{bmatrix} \frac{\partial F}{\partial y_1} & \frac{\partial F}{\partial y_2} & \frac{\partial F}{\partial y_3} & \frac{\partial F}{\partial y_4} & \frac{\partial F}{\partial y_5} & \frac{\partial F}{\partial y_6} & \frac{\partial F}{\partial y_7} \\ \frac{\partial G}{\partial y_1} & \frac{\partial G}{\partial y_2} & \frac{\partial G}{\partial y_3} & \frac{\partial G}{\partial y_4} & \frac{\partial G}{\partial y_5} & \frac{\partial G}{\partial y_6} & \frac{\partial G}{\partial y_7} \\ \frac{\partial H}{\partial y_1} & \frac{\partial H}{\partial y_2} & \frac{\partial H}{\partial y_3} & \frac{\partial H}{\partial y_4} & \frac{\partial H}{\partial y_5} & \frac{\partial H}{\partial y_6} & \frac{\partial H}{\partial y_7} \\ \frac{\partial K}{\partial y_1} & \frac{\partial K}{\partial y_2} & \frac{\partial K}{\partial y_3} & \frac{\partial K}{\partial y_4} & \frac{\partial K}{\partial y_5} & \frac{\partial K}{\partial y_6} & \frac{\partial K}{\partial y_7} \\ \frac{\partial L}{\partial y_1} & \frac{\partial L}{\partial y_2} & \frac{\partial L}{\partial y_3} & \frac{\partial L}{\partial y_4} & \frac{\partial L}{\partial y_5} & \frac{\partial L}{\partial y_6} & \frac{\partial L}{\partial y_7} \\ \frac{\partial M}{\partial y_1} & \frac{\partial M}{\partial y_2} & \frac{\partial M}{\partial y_3} & \frac{\partial M}{\partial y_4} & \frac{\partial M}{\partial y_5} & \frac{\partial M}{\partial y_6} & \frac{\partial M}{\partial y_7} \\ \frac{\partial N}{\partial y_1} & \frac{\partial N}{\partial y_2} & \frac{\partial N}{\partial y_3} & \frac{\partial N}{\partial y_4} & \frac{\partial N}{\partial y_5} & \frac{\partial N}{\partial y_6} & \frac{\partial N}{\partial y_7} \end{bmatrix}, \tag{15}$$

$$\widetilde{\chi} = \begin{bmatrix} 0 & 0 & 1 & 0 & 0 & 0 & 0 \\ 0 & 1 & 0 & 0 & 0 & 0 & 0 \\ -\frac{2y_3}{\Upsilon} & \frac{4y_2+M+\frac{\lambda}{2}-\frac{1}{12}\Upsilon_2(y_3)^2}{\Upsilon} & \frac{-2y_1-\gamma-6\Upsilon_2 y_3 y_2}{\Upsilon} & 0 & 0 & 0 & 0 \\ 0 & 0 & 0 & 0 & 1 & 0 & 0 \\ -\frac{\mathrm{Pr}\, y_5}{\Upsilon_3} & 0 & 0 & 0 & -A^* & 0 & \mathrm{Pr}\, N_B^* y_5 \\ 0 & 0 & 0 & 0 & 0 & 0 & 1 \\ -\frac{Scy_7}{\Upsilon_3} & 0 & 0 & 0 & -B^* & 0 & -\frac{\gamma+Scy_1}{\Upsilon_3} \end{bmatrix}, \tag{16}$$

and

$$\widetilde{\chi} = \begin{bmatrix} 0 & 1 & 0 & 0 & 0 & 0 & 0 \\ 0 & 0 & 1 & 0 & 0 & 0 & 0 \\ 0 & \frac{M+\frac{\lambda}{2}}{\Upsilon} & \frac{-\gamma}{\Upsilon} & 0 & 0 & 0 & 0 \\ 0 & 0 & 0 & 0 & 1 & 0 & 0 \\ 0 & 0 & 0 & 0 & -\frac{\gamma}{\Upsilon_3} & 0 & 0 \\ 0 & 0 & 0 & 0 & 0 & 0 & 1 \\ 0 & 0 & 0 & 0 & \frac{\gamma}{\Upsilon_3}\left(1+\frac{N_{T^*}^*}{N_B^*}\right) & 0 & -\frac{\gamma}{\Upsilon_3} \end{bmatrix}, \tag{17}$$

where

$$A^* = \frac{1}{\Upsilon_3}\left[\gamma - \mathrm{Pr}\,\Upsilon_3\left\{N_B^* y_7 + 2N_{T^*}^* y_5\right\} + \mathrm{Pr}\, y_5\right], \tag{18}$$

$$B^* = \frac{1}{\Upsilon_3}\left[\gamma + \frac{N_{T^*}^*}{N_B^*}\left\{(\gamma - \mathrm{Pr}\,\Upsilon_3\{N_B^* y_7 + 2N_{T^*}^* y_5) + \mathrm{Pr}\, y_5\right\} + Scy_1\right]. \tag{19}$$

The eigen values for Eq. (17) are $\varkappa_1^* = \varkappa_2^* = 1$, $\varkappa_3^* = \varkappa_4^* = 0$, $\varkappa_5^* = -\frac{\gamma}{(\Upsilon)^2}$, $\varkappa_6^* = \varkappa_7^* = -\frac{\gamma}{(\Upsilon_3)^2}$ and the corresponding eigen vector for $\varkappa_1^* = \varkappa_2^* = 1$ is $\widetilde{X} = \begin{bmatrix} 1 & 1 & 0 & 0 & 0 & 0 & 0 \end{bmatrix}^{\check{T}}$. Geometrically, having one or more eigenvalues of zero simply means the null-space is nontrivial, so that the image is a "crushed" a bit, since it is of lower dimension. Since all the parameters are positive this equilibrium has two unstable and two stable eigenvalues. Therefore, we have a saddle at this point $\tilde{O}\,(0,\ 0,\ 0,\ 0,\ 0,\ 0,\ 0)$.

5 Optimal homotopy analysis method

Initial conjectures for dimensionless velocities, temperature and concentration fields corresponding to linear operators are

$$f_0(\xi) = 1 - \frac{1}{e^{\xi}},\ \theta_0(\xi) = e^{-\xi},\ \phi_0(\xi) = e^{-\xi}, \tag{20}$$

$$\mathbb{L}_f = \frac{\mathrm{D}}{\mathrm{D}\xi}\left(\frac{\mathrm{D}^2}{\mathrm{D}\xi^2} - 1\right) f,\ \mathbb{L}_\theta = \left(\frac{\mathrm{D}^2}{\mathrm{D}\xi^2} - 1\right)\theta,\ \mathbb{L}_\phi = \left(\frac{\mathrm{D}^2}{\mathrm{D}\xi^2} - 1\right)\phi, \tag{21}$$

these linear operators observe the following characteristics

$$\mathbb{L}_f\left[\check{D}_1^{**} + \check{D}_2^{**} e^{\xi} + \check{D}_3^{**} e^{-\xi}\right] = 0, \tag{22}$$

$$\mathbb{L}_\theta\left[\check{D}_4^{**} e^{\xi} + \check{D}_5^{**} e^{-\xi}\right] = 0 \tag{23}$$

$$\text{Ł}_{\phi}\left[\check{D}_{6}^{**}e^{\xi}+\check{D}_{7}^{**}e^{-\xi}\right]=0, \tag{24}$$

where $\check{D}_{\hat{J}^*}^{**}\left(\hat{J}^*=1-7\right)$ are the arbitrary constants.

6 Optimal conjunction regulator parameter

The non-zero auxiliary parameters in homotopic solutions standardize the convergence precinct as well as rate of preferred homotopic solutions. To obtain the optimal values of controlling parameters $\hbar_f$, $\hbar_\theta$ and $\hbar_\phi$, we have smeared the perception of minimization by considering the average squared residuals inaccuracies as suggested by Liao [53]:

$$\widetilde{E_m^{*f}}=\frac{1}{\check{c}+1}\sum_{\bar{j}^*=0}^{\check{c}}\left[\bar{N}_f\left(\sum_{\bar{i}^*=0}^{m}\widehat{f}(\xi)\right)_{\xi=\bar{j}^*\delta\xi}\right]^2, \tag{25}$$

$$\widetilde{E_m^{*\theta}}=\frac{1}{\check{c}+1}\sum_{\bar{j}^*=0}^{\check{c}}\left[\bar{N}_\theta\left(\sum_{\bar{i}^*=0}^{m}\widehat{f}(\xi),\ \sum_{\bar{i}^*=0}^{m}\widehat{\theta}(\xi),\ \sum_{\bar{i}^*=0}^{m}\widehat{\phi}(\xi)\right)_{\xi=\bar{j}^*\delta\xi}\right]^2, \tag{26}$$

$$\widetilde{E_m^{*\phi}}=\frac{1}{\check{c}+1}\sum_{\bar{j}^*=0}^{\check{c}}\left[\bar{N}_\phi\left(\sum_{\bar{i}^*=0}^{m}\widehat{f}(\xi),\ \sum_{\bar{i}^*=0}^{m}\widehat{\theta}(\xi),\ \sum_{\bar{i}^*=0}^{m}\widehat{\phi}(\xi)\right)_{\xi=\bar{j}^*\delta\xi}\right]^2. \tag{27}$$

View of Liao's contributions [53]:

$$\widetilde{E_m^{*t}}=\widetilde{E_m^{*f}}+\widetilde{E_m^{*\theta}}+\widetilde{E_m^{*\phi}}, \tag{28}$$

where $\widetilde{E_m^{*t}}$ attitudes for total squared residuals errors, $\delta\xi=0.5$ and $\check{c}=20$. A situation has been reconnoitered where $\Pr=Sc=1.0$, $M=0.5$, $\gamma=0.1$, $\lambda=0.2$, $N_{T^*}^*=0.2$, $N_B^*=0.5$, $\Upsilon_1=0.01$ and $\Upsilon_2=0.02$. It is perceived that at fourth order of approximation, the values of optimal convergent control parameters are $\hbar_f=-0.686219$, $\hbar_\theta=-1.0564$, $\hbar_\phi=-1.99154$ and the total squared residuals error is 0.000476013.

7 Physical quantities of interest

To discuss the fluid flow problems important physical quantaties are Skin friction $\left(\hat{C}_F\right)$, heat transfer coefficient $\left(\check{N}_u\right)$ and mass transfer coefficient $\left(\hat{S}_u\right)$ in dimensional form are defined as:

$$\hat{C}_F=\frac{2\left[\tau_{wall}\right]_{r=R}}{\rho\left(U_w(z)\right)^2},\ \check{N}_u=-\frac{z\left(\frac{\partial T}{\partial r}\right)_{r=R}}{k(T^*-T_\infty^*)},\ \hat{S}_u=-\frac{\left(\frac{\partial C}{\partial r}\right)_{r=R}}{(C^*-C_\infty^*)}, \tag{29}$$

$$\tau_{wall}=\frac{\mu}{2}\frac{\partial u}{\partial z}+\frac{\mu}{2}\frac{\partial w}{\partial r}-\frac{\mu\varepsilon b^2}{12}\left(\frac{\partial u}{\partial z}+\frac{\partial w}{\partial r}\right)\left[2\left(\frac{\partial u}{\partial r}\right)^2+2\left(\frac{\partial w}{\partial z}\right)^2+\left(\frac{\partial u}{\partial z}+\frac{\partial w}{\partial r}\right)^2+2\frac{u^2}{r^2},\right] \tag{30}$$

The dimensionless form is expressed as

$$\hat{C}_F^D = f'' - \frac{\varepsilon}{6}\left[3\left(f'\right)^2 + 3(1+2\gamma\xi)\left(f\right)^2 - 2(1+2\gamma\xi)ff' + (1+2\gamma\xi)(f'')^2\right], \tag{31}$$

$$\check{N}_u^D = -\theta'(0),\ \hat{S}_u^D = -\phi'(0). \tag{32}$$

8 Results and discussion

8.1 Convergence analysis

This portion comprehends the tabular results in the form of error analysis for the convergence of desired homotopic solutions for dimensionless velocity, temperature and concentration. For this analysis we have fixed some tangled parameters and varies one parameter and then we have drafted its behavior. The convergence of desired solution is depicted in Table 1 which confirms that by increasing the order of approximations, error reduces which guaranties the convergence of proposed scheme.

$\check{c}$	$\widetilde{E_{\check{c}}^{*f}}$	$\widetilde{E_{\check{c}}^{*\theta}}$	$\widetilde{E_{\check{c}}^{*\phi}}$
2	2.27231×10^{-2}	3.90068×10^{-2}	1.34981×10^{-2}
4	6.95222×10^{-4}	4.45177×10^{-3}	1.20544×10^{-3}
6	4.19915×10^{-6}	1.36727×10^{-3}	3.94664×10^{-4}
8	7.71003×10^{-7}	5.8439×10^{-4}	1.84679×10^{-4}
10	1.2203×10^{-7}	2.90499×10^{-4}	9.53609×10^{-6}
12	1.51177×10^{-8}	1.60793×10^{-4}	5.37913×10^{-6}
16	1.65518×10^{-9}	6.20223×10^{-6}	2.41867×10^{-6}
20	7.8116×10^{-11}	2.68384×10^{-6}	1.01263×10^{-6}

Table 1: Convergence examination of developed series solutions.

9 Parametric Analysis

The intention of this portion is to inspect the possessions of abundant significant parameters like Sutterby nanofluid parameter (Υ_1), **Darcy** resistance parameter (Υ_2), curvature parameter (γ), magnetic parameter (M), Prandtl number (Pr), Schmidt number (Sc), sponginess parameter (λ), Brownian motion and thermophoresis parameters (N_B^*) and (N_{T^*}) respectively on fluid velocity $f'(\xi)$, temperature $\theta(\xi)$ and concentration $\phi(\xi)$. For this purposes figs. $(2)-(17)$ are sketched.

9.1 Assurance of computed results

Table 2 **is manifested to check the relaince of present results by constructing comparison for the values of skin friction coefficient** $\left(\hat{C}_F^D\right)$ **with published literature presented by Akbar et al.** [55] **and Taimoor et al.** [56] **for different values of magnetic field parameter** (M)**. In order to produce accurate outcome present work is restricted to special case by considering the parameters** $\gamma = \Upsilon_2 = \lambda = N_B^* = \mathrm{Pr} = N_{T^*} = Sc = 0$**. It is found from the obtained values that the**

results are in total covenant with each other. Furthermore the compatibility of current work is done by establishing the comparison for heat transfer coefficient by considering $\gamma = \Upsilon_2 = \lambda = N_B^* = M = N_T^* = Sc = 0$. **It is worthy to mention that by restricting these parameter to zero present investigation reduces to heat transfer in a fluid flow over a stretching sheet. From the attained numerical data explicated in** Table 2 **it is concluded that result are matching in excellent way.**

9.2 Bearing of influential variables on velocity field

Effects of velocity $f'(\xi)$ is visualized through figs. $(2)-(6)$ and behavior of the involved parameters is censored through these graphs. Effect of magnetic parameter (M) is drafted in fig. 2. It is depicted that $f'(\xi)$ decreases by increasing (M). It is due to the reason that magnetic parameters in the dimensionless equations appears due to Lorentz force term which is resistive force in nature. Variation of porosity parameter (λ) is envisioned through fig. 3. It has been observed that $f'(\xi)$ is the decreasing function of porosity parameter (λ). Fig. 4 shows the effects of curvature parameter (γ) on the velocity profile $f'(\xi)$. It shows that $f'(\xi)$ is the decreasing function of curvature parameter (γ). Fig. 5 is portraying the impact of Sutterby nanofluid parameters (Υ_1) on $f'(\xi)$. It is depicted that fluid velocity $f'(\xi)$ decelerates as we increase Sutterby nanofluid parameters (Υ_1). Fig. 6 is plotted to notice the influence of **Darcy** parameter (Υ_2) on $f'(\xi)$. It is noted that fluid accelerates as the values of **Darcy** parameter (Υ_2) are increased.

9.3 Scrutiny of involved variables on temperature field

Influence of different involved parameters on dimensionless temperature field $\theta(\xi)$ have been demonstrated through figs. $(7)-(10)$. In fig. 7 variation of porosity parameter (γ) is sketched. It is depicted that as we increase the porosity parameter (γ), corresponding temperature field $\theta(\xi)$ and associated thermal layer thickness increases. Deviation of Prandtl number (Pr) on non-dimensional temperature is portrayed in fig. 8. It reveals that as we increase the Prandtl number (Pr), corresponding temperature field $\theta(\xi)$ and thermal boundary layer reduces. It is due to the fact that Prandtl number (Pr) has an inverse relation to thermal diffusion. Fig. 9 is plotted to examine the behavior of Brownian motion parameter (N_B^*) to temperature field $\theta(\xi)$. It is observed that Brownian motion parameter (N_B^*) has a direct relation to temperature field $\theta(\xi)$ meaning that by increasing the Brownian motion parameter (N_B^*), non-dimensional temperature increases. Deviation of thermophoresis parameter (N_T^*) is studied through fig. 10. It is scrutinized that increasing values of thermophoresis parameter $(N_{T^*}^*)$ corresponds to increase in temperature field $\theta(\xi)$ and thermal boundary layer thickness.

9.4 Visualization of involved variables on concentration solution

In figs. $(11)-(14)$ behavior of some involved parameter on non-dimensional concentration field $\phi(\xi)$ and solutal layer thickness is portrayed. Fig. 11 is delineated to inspect the influence of Schmidt number (Sc) on concentration field $\phi(\xi)$. It is scrutinized that increasing values of Schmidt number (Sc) corresponds to decrease in mass diffusion (D_m) and due to this concentration field $\phi(\xi)$ reduces. Fig. 12 is plotted for non-dimensional concentration field $\phi(\xi)$ against curvature parameter (γ). It is professed that non-dimensional concentration $\phi(\xi)$ decelerates by growing curvature parameter (γ). Fig. 13 is plotted to detect that how concentration field $\phi(\xi)$ gets affected with the variation of thermophoresis parameter $(N_{T^*}^*)$.

It has been pointed that involvement of increasing values of thermophoresis parameter (N_{T*}^{*}) corresponds to increase the concentration field $\phi(\xi)$. Fig. 14 is strategized to scrutinize that how dimensionless concentration acts when Brownian motion parameter (N_{B}^{*}) increases. It portrays that Brownian motion parameter (N_{B}^{*}) is the diminishing function of dimensionless concentration field $\phi(\xi)$ and associated boundary layer thickness.

Figs. 15 and 16 are plotted for the stream lines pattern of dimensionless velocities in the form of stream plot and density plot. It is observed that streamlines for the Sutterby fluid model shows curvilinear behavior. Fig. 17 depicts the phase portrait of velocity.

M	Akbar et al. [55]	Taimoor et al. [56]	Present Results
0	1	1	1
0.5	−1.11803	−1.11802	−1.11800
1	−1.41421	−1.41419	−1.41420
5	−2.44949	−2.44945	−2.44947

Table 2: Comparison of skin friction coefficeint $(\hat{C}_{F}^{D})$ with previous published results [55] **and** [56].

γ	Rangi and Naseem [57]	Present results
0.0	−0.985286	−0.985287
0.25	−1.079447	−1.079444
0.5	−1.173899	−1.173900
0.75	−1.267214	−1.267210
1.0	−1.359308	−1.359305

Table 3: Comparison of Nusselt number $-\theta'(0)$ with previous published results [57].

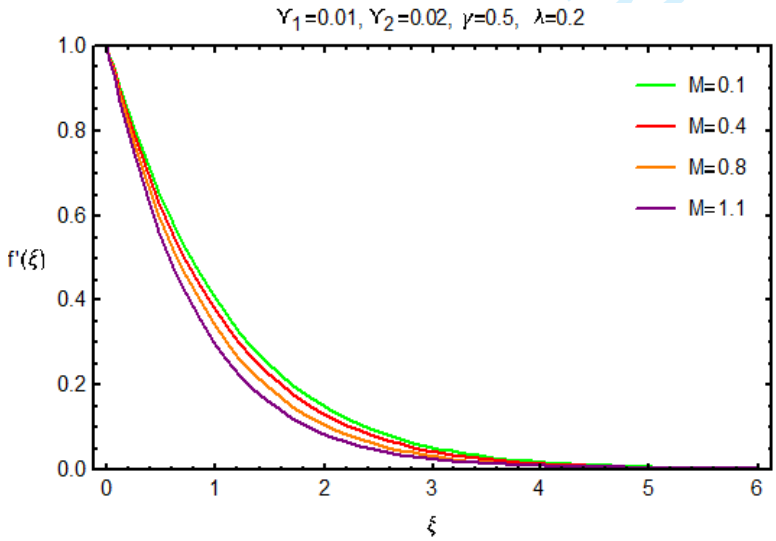

Fig. 2: Variation of M on $f'(\xi)$.

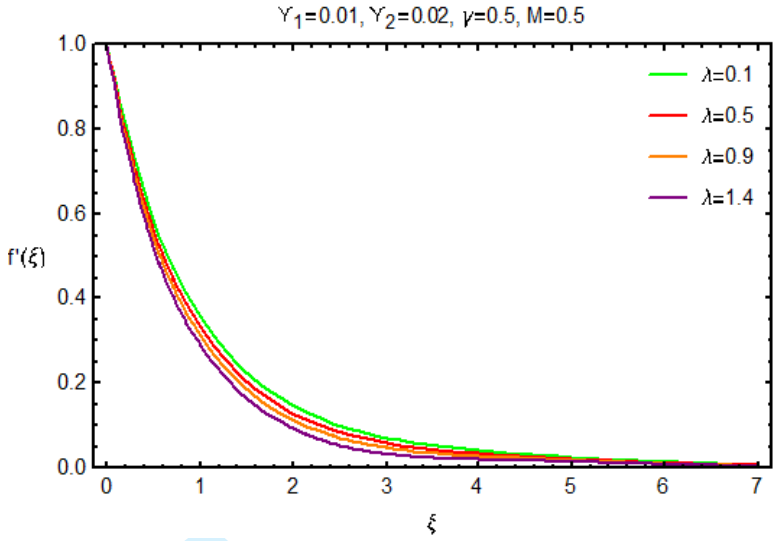

Fig. 3: Variation of λ on $f'(\xi)$.

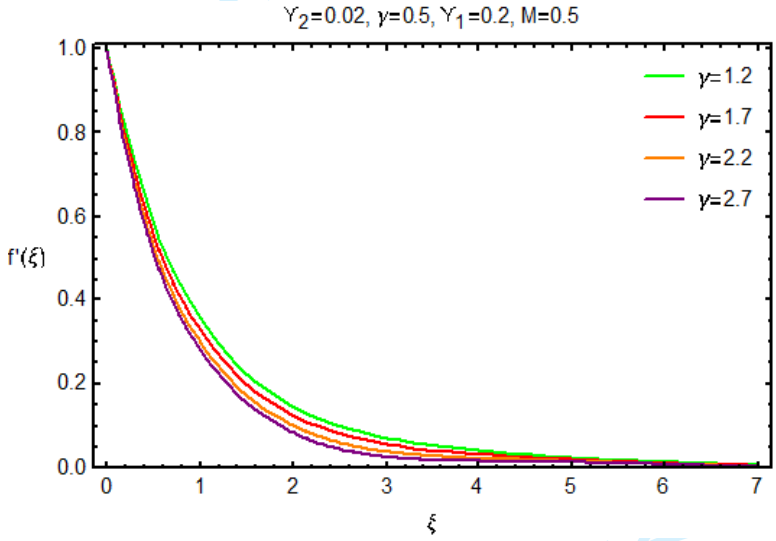

Fig. 4: Variation of γ on $f'(\xi)$.

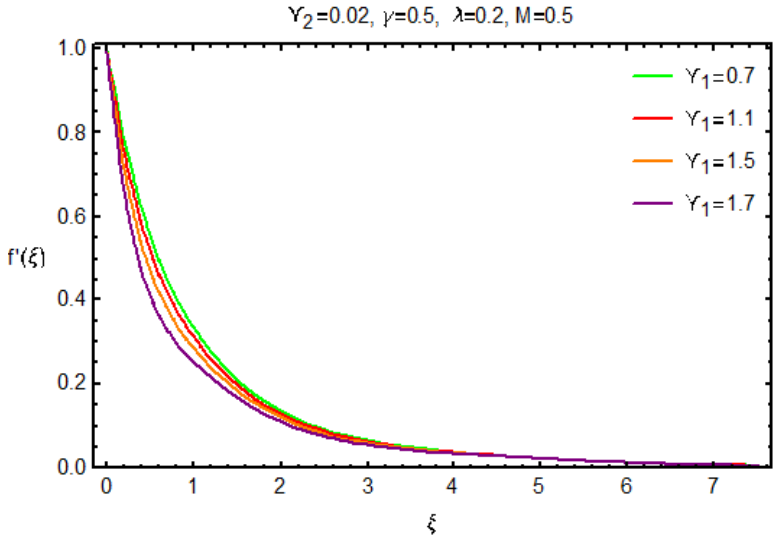

Fig. 5: Variation of γ_1 on $f'(\xi)$.

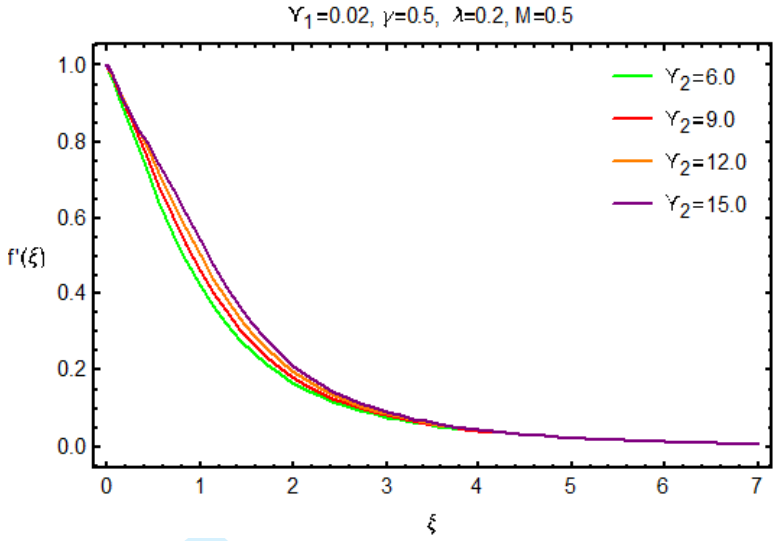

Fig. 6: Variation of γ_2 on $f'(\xi)$.

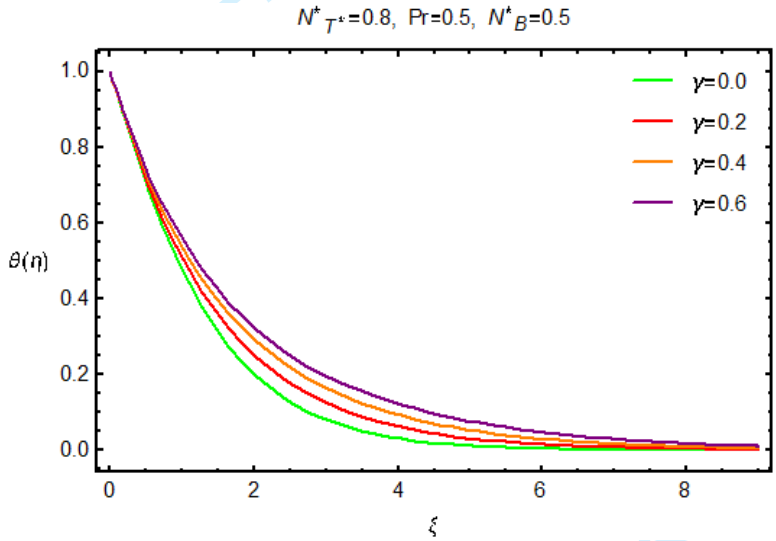

Fig. 7: Variation of γ on $\theta(\xi)$.

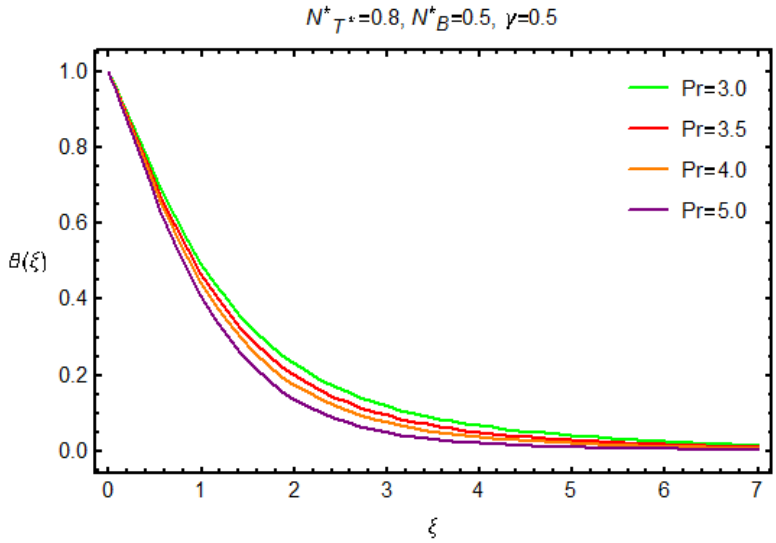

Fig. 8: Variation of Pr on $\theta(\xi)$.

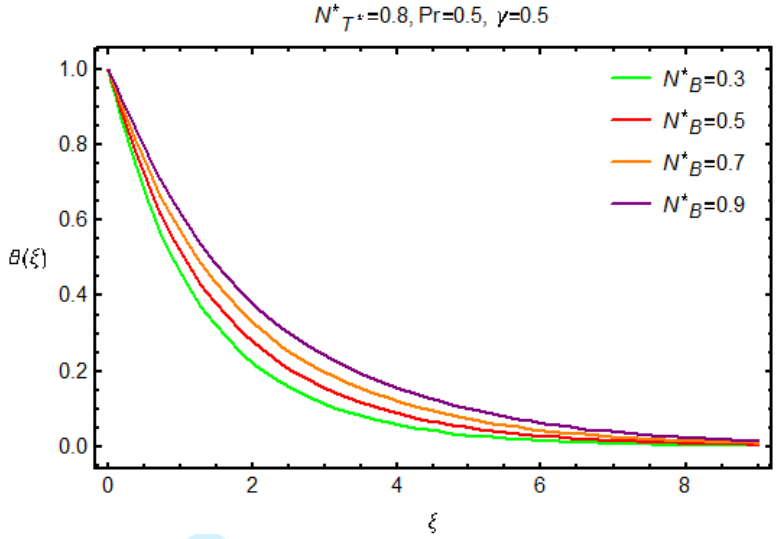

Fig. 9: Variation of N_B^* on $\theta(\xi)$.

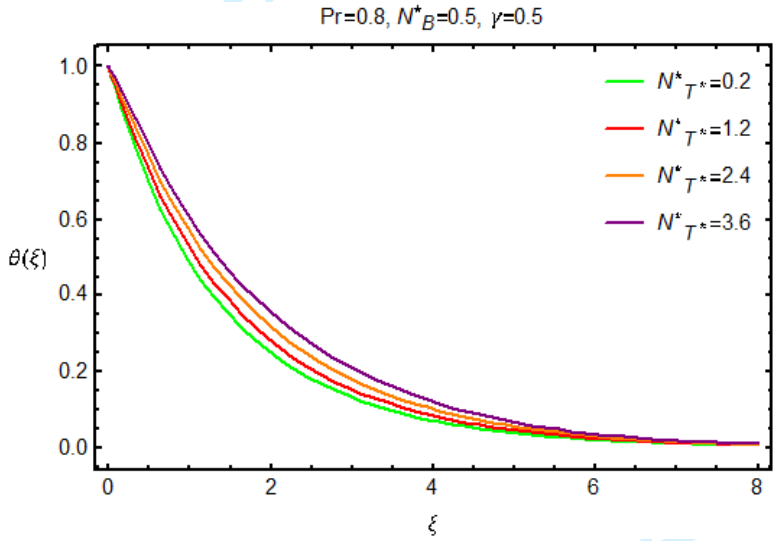

Fig. 10: Variation of N_{T*}^* on $\theta(\xi)$.

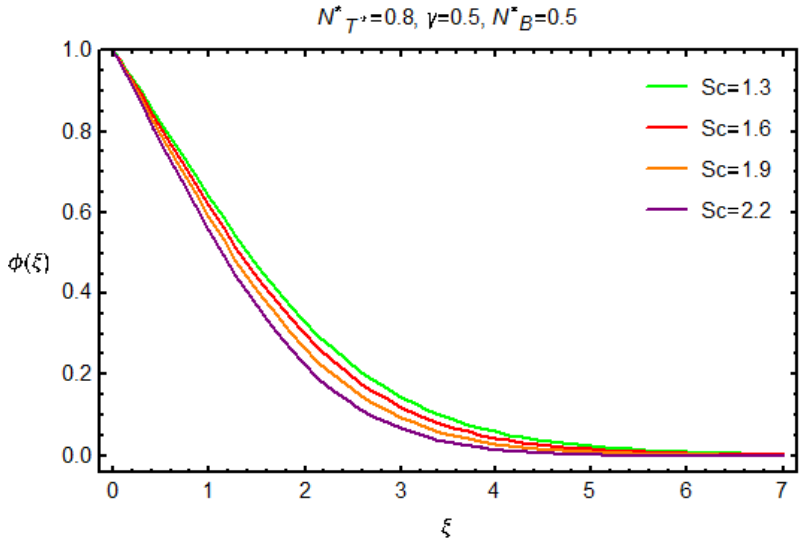

Fig. 11: Variation of Sc on $\phi(\xi)$.

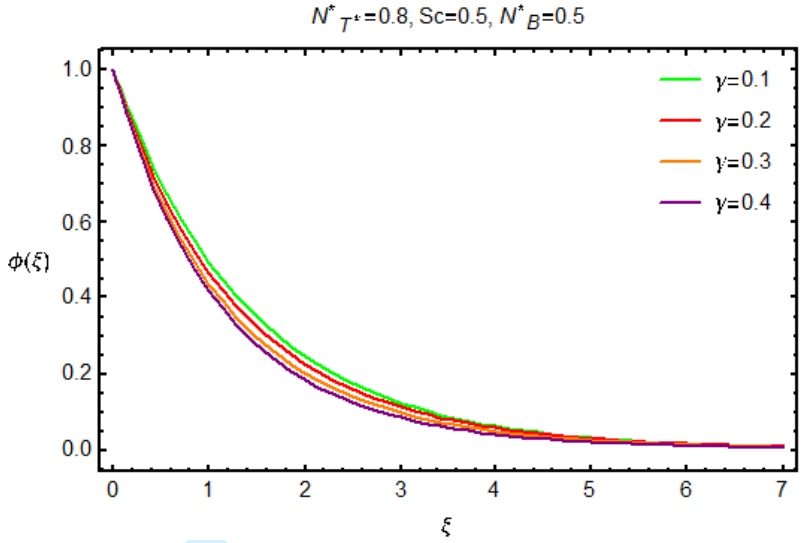

Fig. 12: Variation of γ on $\phi(\xi)$.

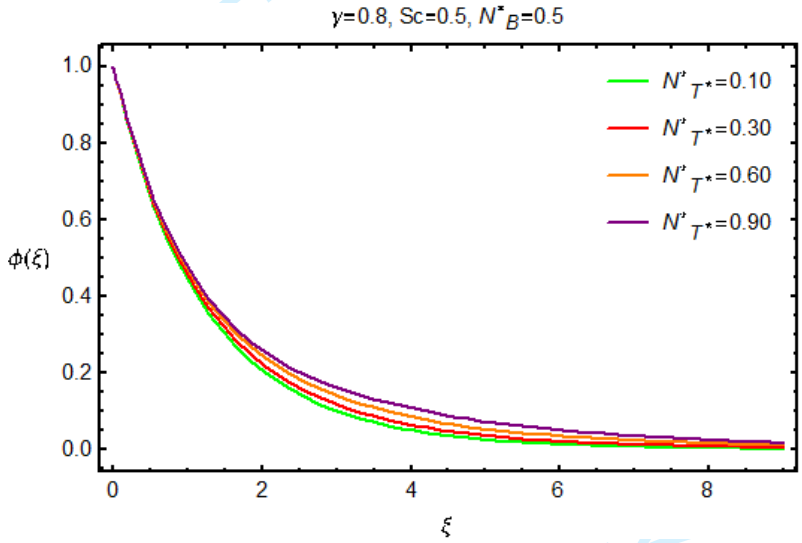

Fig. 13: Variation of $N_{T^*}^*$ on $\phi(\xi)$.

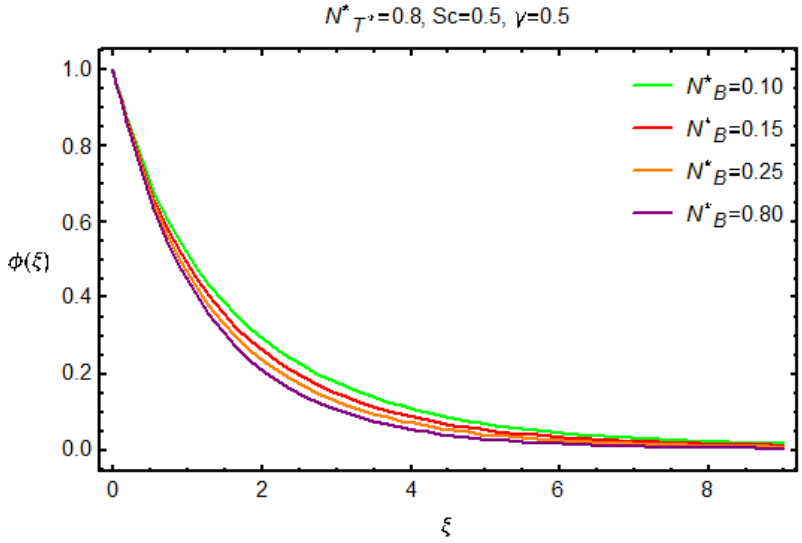

Fig. 14: Variation of N_B^* on $\phi(\xi)$.

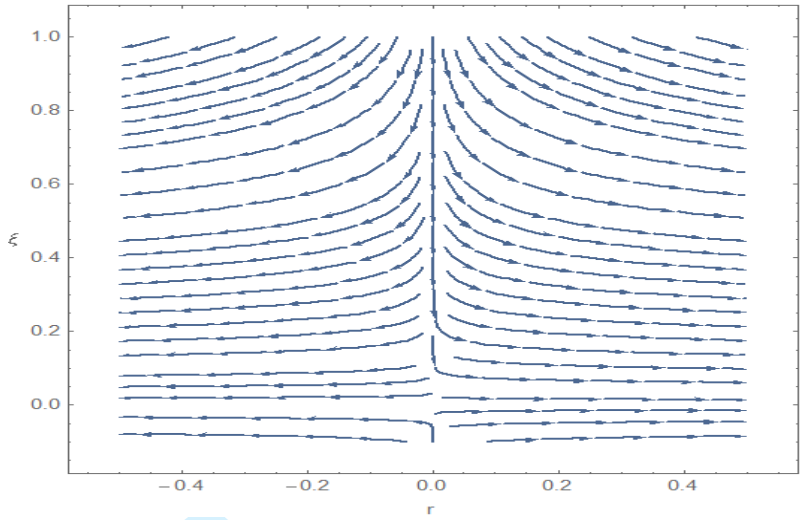

Fig. 15: Stream lines for velocities.

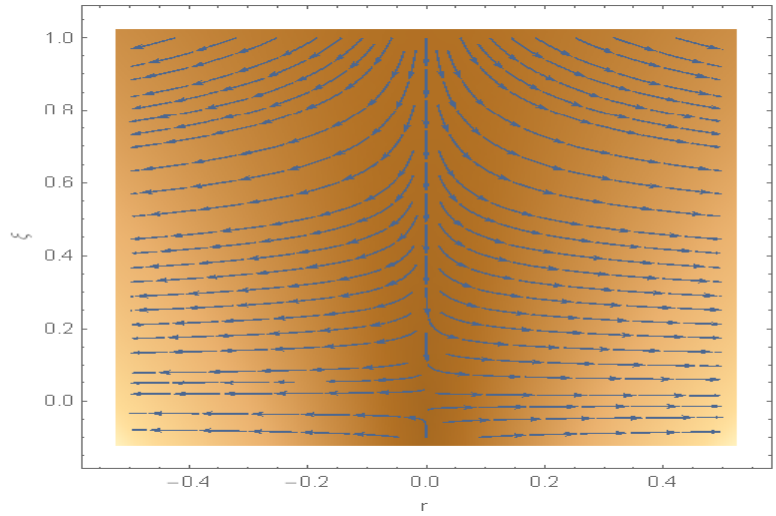

Fig. 16:Stream density plot for velocity.

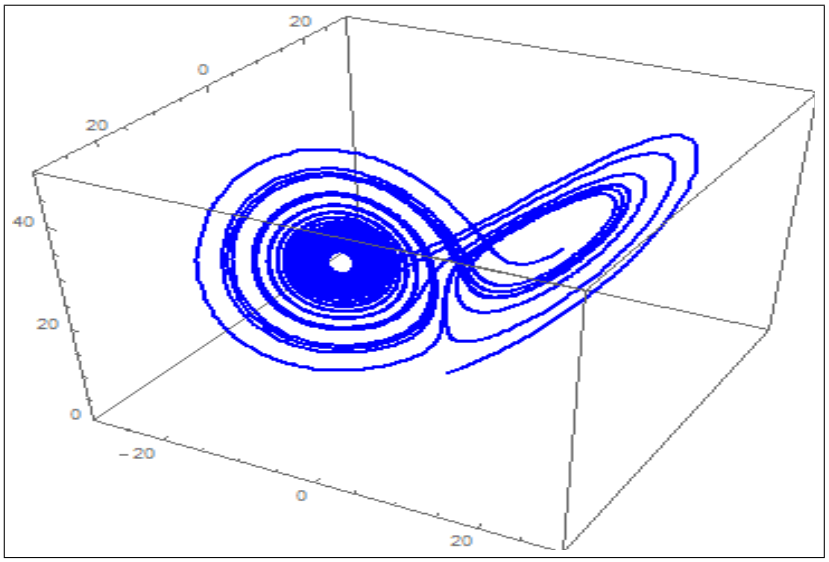

Fig. 17:Phase portrait in three dimensions.

10 Concluding Remarks of present exploration

Two-dimensional MHD boundary layer flow of steady, incompressible Sutterby nanofluid by stretching cylinder are inspected in this study. From the contemporary investigations, the main interpretations were as follows:

- Non-dimensional velocity $f'(\xi)$ shows decreasing nature for magnetic parameter (M), porosity parameter (λ), curvature parameter (γ), Sutterby fluid parameter (Υ_1), and shows the reverse behavior for **Darcy** resistance parameter (Υ_2).
- An increase in Schmidt number (Sc) and thermophoresis parameter (N_{T*}^*) on concentration field shows reverse behavior to concentration and solutal layer thickness.
- Prandtl number (Pr) corresponds to decreasing behavior of non-dimensional temperature field and associated boundary layer thickness decreases.
- Both temperature and concentration fields increases by enhancing thermophoresis parameter (N_{T*}^*).
- Effect of Brownian motion parameter (N_B^*) on fluid temperature and concentration behaves opposite to each other.
- Both temperature and concentration fields increases by increasing magnetic parameter (M) and their associated boundary layer thickness.
- Curvature parameter (γ) depicts opposite behavior to fluid temperature and concentration and as well on their associated boundary layer thickness.

References

[1] S. U. S. Choi, Enhancing thermal conductivity of fluids with nanoparticles. ASME Institute of Mechcanica Engineering, **66**, 99 (1995).

[2] H. Masuda, A. Ebata, K. Termae and N. Hishinunmah, Alteration of thermal conductivity and viscosity of liquid by dispersing ultra-fine particles, Netsu Bussei, **7**, 227 (1993) .

[3] J. Buongiorno, Convective transport in nanofluids, ASME J. Heat Transf., **128**, 240 (2006).

[4] D. A. Nield and A. V. Kuznestov, The Cheng-Minkowycz problem for natural convective boundary-layer flow in a porous medium saturated by a nanofluid, Int. J. Heat Mass Transf., **52**, 5792 (2009).

[5] **M. Sheikholeslami, S. A. Shehzad and S. Li, Water based nanofluid free convection heat transfer in a three dimensional porous cavity with hot sphere obstacle in existence of Lorentz forces, Int. J. Heat Mass Transf., 125, 375 (2018).**

[6] **M. Sheikholeslami, S. A. Shehzad, F. M. Abbasi and Z. LI, Nanofluid flow and forced convection heat transfer due to Lorentz forces in a porous lid driven cubic enclosure with hot obstacle, Comput. Methods Appl. Mech. Eng., 338, 491 (2018).**

[7] **M. Sheikholeslami and A. Zeeshan, Analysis of flow and heat transfer in water based nanofluid due to magnetic field in a porous enclosure with constant heat flux using CVFEM, Comput. Methods Appl. Mech. Eng., 320, 68 (2017).**

[8] **M. Sheikholeslami, M. Jafaryar and Z. Li, Second law analysis for nanofluid turbulent flow inside a circular duct in presence of twisted tape turbulators, J. Mol. Liq., 263, 489 (2018).**

[9] **M. Sheikholeslami, S. A. Shehzad, F. M. Abbasi and A. Shafee, Numerical modeling for alumina nanofluid magnetohydrodynamic convective heat transfer in a permeable medium using Darcy law, Int. J. Heat Mass Transf., 127, 614 (2018).**

[10] W. A. KHAN and I. POP, Boundary-layer flow of a nanofluid past a stretching sheet, Int. J. Heat Mass Transf., **53**, 2477 (2010).

[11] M. M. Rahman, A. V. Rosca and I. POP, Boundary layer flow of a nanofluid past a permeable exponentially shrinking/stretching surface with second order slip using Buongiorno's model, Int. J. Heat Mass Transf., **77**, 1133 (2014) .

[12] C. Zhang, L. Zheng, X. Zhang and G. Chen, MHD flow and radiation heat transfer of nanofluids in porous media with variable surface heat flux and chemical reaction, Appl. Math. Model., **39**, 161 (2015).

[13] S. Nadeem, R. Ul. Haq and Z. H. Khan, Numerical study of MHD boundary layer flow of Maxwell fluid past a stretching sheet in the presence of nanoparticles, J. Taiwan Inst. Chem. Eng., **45**, 121 (2014) .

[14] M. Y. Malik, I. Khan, A. Hussain and T. Salahuddin, Mixed convection flow of MHD Eyring-Powell nanofluid over a streching sheet: A numerical study, AIP Adv., **5**, 117118 (2015) .

[15] C. S. K. Raju and N. Sandeep, Unsteady Casson nano over a rotating cone in a rotatingframe filled with ferrous nanoparticles: A numerical study, J. Magn. Magn. Mater., **421**, 216 (2017) .

[16] S. Nadeem and S. Saleem, Analytical study of third grade fluid over a rotating vertical cone in the presence of nanoparticles, Int. J. Heat Mass Transf., **85**, 1041 (2015).

[17] C. S. K. Raju, N. Sandeep and A. Malvandi, Free convective heat and mass transfer of MHD Non-Newtonian nanofluids over a cone in the presence of non-uniform heat soure/sink, J. Mol. Liq., **221**, 108 (2016) .

[18] S. Nadeem and S. Saleem, Unsteady mixed convection flow of nanofluid on a rotating cone with magnetic field, Appl. Nanosci., **4**, 405 (2014) .

[19] S. Nadeem and S. Saleem, Analytical Study of Rotating Non-Newtonian nanofluid on a Rotating Cone, J. Thermophys. Heat Transf., **28**, 295 (2014) .

[20] S. Nadeem, R. Ul. Haq and Z. H. Khan, Numerical solution of non-Newtonian nanofluid flow over a stretching sheet, Appl. Nanosci., **4**, 625 (2014) .

[21] **M. Sheikholeslami, Z. Lee and A. Shafee, Lorentz forces effect on NEPCM heat transfer during solidification in a porous energy storage system, Int. J. Heat Mass Transf., 127, 665 (2018).**

[22] **M. Sheikholeslami, Influence of magnetic field on Al2O3-H2O nanofluid forced convection heat transfer in a porous lid driven cavity with hot sphere obstacle by means of LBM, J. Mol. Liq., 263, 472 (2018).**

[23] W. A. Khan, O. D. Makinde and Z. H. Khan, Non-aligned MHD stagnation point flow of variable viscosity nanofluids past a stretching sheet with radiative heat, Int. J. Heat Mass Transf., **96**, 525 (2016) .

[24] T. Hayat, M. B. Ashraf, S. A. Shehzad and A. Alsaedi, Mixed convection flow of Casson nanofluid over a stretching sheet with convectively heated chemical reaction and heat source/sink, J. Appl. Fluid Mech., **8**, 803 (2015).

[25] **M. Sheikholeslami, Application of Darcy law for nanofluid flow in a porous cavity under the impact of Lorentz forces, J. Mol. Liq., 266, 495 (2018).**

[26] **M. Sheikholeslami, Finite element method for PCM solidification in existence of CuO nanoparticles, J. Mol. Liq., 265, 347 (2018).**

[27] **M. Sheikholeslami, Solidification of NEPCM under the effect of magnetic field in a porous thermal energy storage enclosure using CuO nanoparticles, J. Mol. Liq., 263, 303 (2018).**

[28] **M. Sheikholeslami and H. B. Rokni, CVFEM for effect of Lorentz forces on nanofluid flow in a porous complex shaped enclosure by means of non-equilibrium model, J. Mol., Liq., 254, 446 (2018).**

[29] **M. Sheikholeslami, CuO-water nanofluid flow due to magnetic field inside a porous media considering Brownian motion, J. Mol., Liq., 249, 921 (2018) .**

[30] **M. Sheikholeslami and H. B. Rokni, Magnetic nanofluid flow and convective heat transfer in a porous cavity considering Brownian motion effects, Phy. Fluid, 30, 10.1063/1.5012517 (2018).**

[31] T. Hayat, S. Ayub, A. Alsaedi, A. Tanveer and B. Ahmad, Numerical simulation for peristaltic activity of Sutterby fluid with modified Darcy's law, Res. Phys., **7**, 762 (2017).

[32] A. Guha and K. Pradhan, Natural convection of non-Newtonian power law fluids on a horizontal plate, Int. J. Heat Mass Transf., **70**, 930 (2014).

[33] S. Bijjan, A. Dihman and V. Gautam, Laminar momentum and heat transfer phenomenon of power law dilatant fluid around an asymmetrically confined cylinder, Int. J. Therm. Sci., **88**, 110 (2015).

[34] E. Azhar, Z. Iqbal and E. N. Maraj, Impact of entropy generation on stagnation point flow of Sutterby nanofluid: a numerical analysis, De Gruyter. Z Naturforsch, **71**, 837 (2016).

[35] T. Hayat, H. Zahir, M. Mustafa and A. Alsaedi, Peristaltic flow of Sutterby fluid in a vertical channel with radiative heat transfer and compliant walls: a numerical study, Res. Phys., **6**, 805 (2016).

[36] Z. Y. Xie and Y. J. Jian, Rotating electromagnetohydrodynamics flow of power law fluid through a micro parallel channel, Colloids Surf. A, **529**, 334 (2017).

[37] T. Hayat, S. Ayub, A. Alsaedi, A. Tanveer and B. Ahmad, Numerical simulation for peristaltic activity of Sutterby fluid with modified Darcy's law, Res. Phys., **7**, 762 (2017).

[38] T. Hayat, Quratulain, F. Alasadi, M. Rafiq and B. Ahmad, On effects of thermal radiation and radial magnetic field for peristalsis of Sutterb liquid in a curved channel with wall properties, Chin. J. Phys., **55**, 2005 (2017).

[39] K. B. Pavlov, Magnetohydrodynamic flow of an incompressible viscous fluid caused by deformation of a plane surface, Magnitnaya Gidrodinamika, **4**, 146 (1974).

[40] A. Ishak, R. Nazar and I. POP, Magnetohydrodynamic (MHD) flow and heat transfer due to a stretching cylinder, Energy Convers. Manag., **49**, 3265 (2008).

[41] **M. Sheikholeslami and H. B. Rokni, Numerical modeling of nanofluid natural convection in a semi annulus in existence of Lorentz force, Comput. Methods Appl. Mech. Eng., 317, 419 (2017).**

[42] O. D. Makinde and W. N. Mutuku, Hydromagnetic thermal boundary layer of nanofluids over a convectively heated flat plate with viscous dissipation and Ohmic heating, UPB Scientific Bulletin, Series A, **76**, 181 (2014) .

[43] **M. Sheikholeslami and K. Vajravelu, Nanofluid flow and heat transfer in a cavity with variable magnetic field, Appl. Math. Comput., 298, 272 (2017).**

[44] S. Singh and O. D. Makinde, Computational dynamics of MHD free convection flow along an inclined plate with Newtonian heating in the presence of volumetric heat generation, Chem. Eng. Commun., **199**, 1144 (2012).

[45] S. Singh and O. D. Makinde, Axisymmetric slip flow on a vertical cylinder with heat transfer, Sains Malaysiana, **43** 483 (2014).

[46] S. Das, R. N. Jana and O. D. Makinde, MHD Boundary layer slip flow and heat transfer of nanofluid past a vertical stretching sheet with non-uniform heat generation/ absorption, Int. J. Nanosci., **13**, 1 : 12 1450019(2014).

[47] S. Mukhopadhayay, M. A. G. Arif and M. P. A. Wazed, MHD boundary layer flow along a stretching cylinder, Acta Technica, **58**, 3 (2013) .

[48] M. Qasim, Z. H. Khan, W.A. Khan and I. A. Shah, MHD boundary layer slip flow and heat transfer of ferrofluid along a stretching cylinder with prescribed heat flux, PLoS One, **9**, (2014).

[49] M. Y. Malik, T. Salahuddin, A. Hussain and S. Bilal, MHD flow of tangent hyperbolic fluid over a stretching cylinder: using Keller box method, J. Magn. Magn. Mater., **395**, 271 (2015).

[50] J. Benazir, R. Sivaraj and O. D. Makinde, Unsteady magnetohydrodynamic Casson fluid flow over a vertical cone and flat plate with non-uniform heat source/ sink. Int. J. Eng. Res. Africa, **21**, 69 (2016) .

[51] S. J. Liao, Homotopy Analysis Method in Nonlinear Differential Equations, Springer and higher education press, Heidelberg, (2012).

[52] U. Farooq, Y. L. Zhao, T. Hayat, A. Alsaedi and S. J. Liao, Application of the HAM-based mathematica package BVPh 2.0 on MHD Falkner-Skan flow of nanofluid, Comput. Fluids, **111**, 69 (2015).

[53] S. J. Liao, An optimal Homotopy analysis approach for strongly nonlinear differential equations, Comm. Nonlinear Sci. Numer. Simul., **15**, 2003 (2010).

[54] A. Raees, H. Xu, H and S. J. Liao, Unsteady mixed nano-bioconvection flow in a horizontal channel with its upper plate expanding or contracting, Int. J. Heat Mass Transf., **86**, 174 (2015) .

[55] N. S. Akbar, A. Ebai and Z. H. Khan, Numerical analysis of magnetic field effects on Eyring–Powell fluid flow towards a stretching sheet, J. Magn. Magn. Mater., **382**, 355 (2015).

[56] M. Y. Malik, T. Salahuddin, A. Hussain and S. Bilal, MHD flow of tangent hyperbolic fluid over a stretching cylinder: Using Keller box method, J. Magn. Magn. Mater., **395**, 271 (2015).

[57] R. R. Rangi and N. Ahmad, Boundary Layer Flow past a Stretching Cylinder and Heat Transfer with Variable Thermal Conductivity, Applied Mathematics, **3**, 205 (2012).